

System design and development of a pinhole SPECT system for quantitative functional imaging of small animals

Toshiyuki AOI,^{*,**} Tsutomu ZENIYA,^{*} Hiroshi WATABE,^{*} Hossain M. DELOAR,^{*}
Tetsuya MATSUDA^{**} and Hidehiro IIDA^{*}

^{*}Department of Investigative Radiology, National Cardiovascular Center Research Institute

^{**}Department of System Science, Graduate School of Informatics, Kyoto University

Recently, small animal imaging by pinhole SPECT has been widely investigated by several researchers. We developed a pinhole SPECT system specially designed for small animal imaging. The system consists of a rotation unit for a small animal and a SPECT camera attached with a pinhole collimator. In order to acquire complete data of the projections, the system has two orbits with angles of 90° and 45° with respect to the object. In this system, the position of the SPECT camera is kept fixed, and the animal is rotated in order to avoid misalignment of the center of rotation (COR). We implemented a three dimensional OSEM algorithm for the reconstruction of data acquired by the system from both the orbitals. A point source experiment revealed no significant COR misalignment using the proposed system. Experiments with a line phantom clearly indicated that our system succeeded in minimizing the misalignment of the COR. We performed a study with a rat and ^{99m}Tc-HMDP, an agent for bone scan, and demonstrated a dramatic improvement in the spatial resolution and uniformity achieved by our system in comparison with the conventional Feldkamp algorithm with one set of orbital data.

Key words: pinhole SPECT, complete data acquisition, small animal imaging

INTRODUCTION

IN VIVO IMAGING of physiological functions (e.g., the tissue blood flow and receptor binding potentials) in small laboratory animals facilitates the objective assessment of pharmaceutical development and regenerative therapy in pre-clinical trials. Micro positron emission tomography (PET) has been extensively emphasized for achieving high spatial resolution in the imaging of small animals, which approaches 1.0 mm.^{1–3} An alternative methodology for small animal imaging is micro single photon emission computed tomography (micro SPECT) in which a camera is fitted with a pinhole collimator.^{4–8} Pinhole

SPECT has low sensitivity as compared with small animal PET; however, depending on the size of the pinhole, the spatial resolution achieved by pinhole SPECT can exceed that of PET. Unlike PET systems, the pinhole SPECT system does not require a cyclotron for producing radiopharmaceuticals, and it has an excellent cost/performance ratio. Moreover, the half life of radiopharmaceuticals used for pinhole SPECT is relatively longer than that used for PET, which is beneficial in investigating slow pharmacokinetics.

In addition to the lower sensitivity of pinhole SPECT, the existence of image distortion in the axial direction and non-uniform spatial resolution in the reconstructed image for the pinhole SPECT are also areas of concern. One explanation for this non-uniformity is due to incompleteness of data and use of Feldkamp filtered backprojection (FBP) algorithm as an approximate 3D FBP.⁹ This non-uniformity can be suppressed by applying statistical reconstruction algorithms such as maximum likelihood expectation maximization (MLEM)^{10,11} or ordered subsets expectation maximization (OSEM),¹² but in the periphering of FOV, the

Received June 30, 2005, revision accepted December 13, 2005.

For reprint contact: Toshiyuki Aoi, R.T., Department of Investigative Radiology, National Cardiovascular Center Research Institute, 5–7–1 Fujishiro-dai, Suita, Osaka 565–8565, JAPAN.

E-mail: toshiaoi@ri.ncvc.go.jp

image is blurred.^{5,13} This non-uniformity of the image resolution often hampers further quantitative analysis. Tuy showed that in order to obtain a strict three-dimensional (3D) tomogram in cone-beam CT, the following geometric condition should be fulfilled: “all the planes that cross an object cross the axis of the X-ray source.”^{14,15} Tuy’s condition can be adapted to pinhole SPECT. The conventional pinhole SPECT with one circular orbit does not fulfill this condition. Kudo and Saito suggested examples of orbits that can satisfy Tuy’s condition: use of two circular orbits, a spiral orbit, or a single circular orbit in conjunction with a straight line.^{16–18} By satisfying Tuy’s condition, Zeniya et al. demonstrated an improvement in the uniformity of the spatial resolution of pinhole SPECT by using two circular orbits with angles of 90° and 45° with respect to the object.¹⁹ However, they did not present details of a system configuration including hardware and software. In this paper, we focused on the detailed descriptions of system (hardware as well as software) which is able to properly acquire data from two circular orbits.

MATERIALS AND METHODS

System configuration

The misalignment of the center of rotation (COR) could be more critical for data acquisition with two orbits as compared with a single orbital system. Therefore, in the proposed system, the detector and collimator were fixed, and the small animal was rotated. The outline of the system and the data flowchart are shown in Figure 1. This system consists of a rotation unit (RU), rotation unit control board (RU controller), pinhole collimator, and SPECT camera.

Rotation unit (RU)

A small animal was rotated on the RU (Fig. 2), which consisted of a base-board and a rotating stage. The rotating stage was driven by a stepping motor (SGSP-120YAW- θ z, Sigma Company, Tokyo, Japan) with a COR accuracy of 20 μ m. As shown in Figure 2, the small animal can be fixed in the direction of either 90° or 45°. The axes of the two directions intersect each other, and the distances between the intersection point and each base are equal ($T1 = T2$). In order to perform data acquisition with two circular orbits, the intersection point must coincide with the COR of the pinhole detector, i.e., the line perpendicular to the detector center should cross the intersection point, as shown in Figure 2. An adjustment implement (Fig. 3) was utilized to achieve this. The implement was designed to position a radioactive point source at the COR. Then, the COR was adjusted by acquiring data with the point source for various angle directions.

The rat holder was prepared such that the femoral parts and tail of the rat would lie out of the holder (Fig. 4). It was fabricated from 0.5 mm-thick vinyl chloride.

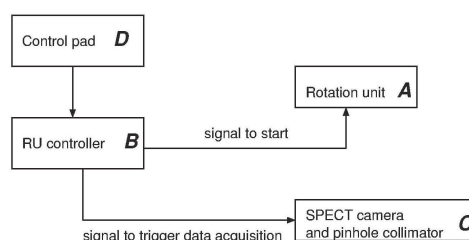
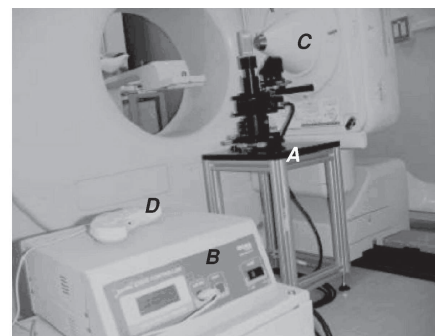


Fig. 1 Upper: Overview of the proposed pinhole SPECT system for small animals. Lower: Schematic diagram of the system. (A) rotation unit (RU), (B) RU controller, (C) SPECT camera and pinhole collimator, and (D) control pad.

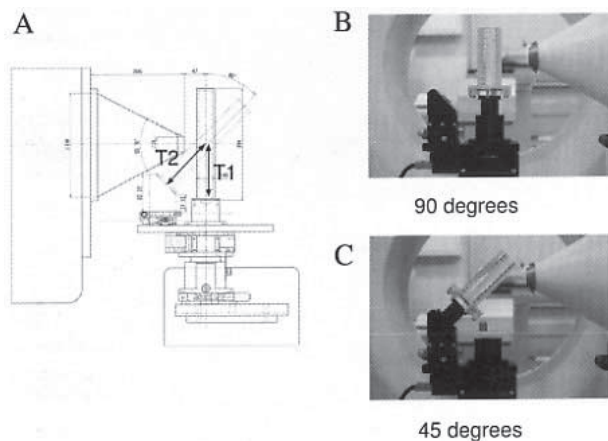


Fig. 2 Cross section of the rotation unit (A) and schematic views of the 90° orbit (B) and 45° orbit (C).

RU controller

In order to control the RU, a general-purpose controller (Mark202, Sigma Company, Tokyo, Japan) was employed. The RU controller could control the starting point of the stepping motor, rotation direction, step angle, and speed of rotation using a control pad. The minimum amount of movements per pulse was 0.01° and the maximum speed of movement was 100°/s.

Pinhole collimator

The pinhole collimator (NDCL709A, Toshiba, Tokyo, Japan) used had a tungsten knife-edge head, which was replaceable. The available hole sizes were 0.25 mm, 0.5

$$\lambda_j^{k+1} = \frac{\lambda_j^k}{\sum_{l=1}^2 \sum_{i=1}^n c_{lij}} \sum_{l=1}^2 \sum_{i=1}^n \frac{y_{li} c_{lij}}{\sum_{j=1}^m c_{lij} \lambda_j^k} \quad (5)$$

where, as shown in Figure 5, λ_{jk} is the value of the image voxel j for the k -th iteration, y_{li} is the measured value of the projection pixel i for the l -th orbit, and c_{lij} is the probability of detecting a photon originating from image voxel j at projection pixel i for the l -th orbit.

Here, we used an OS scheme¹² to reduce the number of iterations. Subsets were evenly divided from both orbits for the OS scheme. A 3D voxel-driven projector using bilinear interpolation on the detector plane was employed in both forward- and back-projections. While back-projecting, the projection data from different orbits were transformed into the same coordinate and combined in the reconstructed 3D matrix space. The software was implemented on a 2.4-GHz PC with Xeon CPU and 1 GB of physical memory, running on a Linux operating system (version 2.4.18).

Experiment with a point source

In order to validate whether the projection data from two orbits were correctly acquired, we performed an experiment using a radioactive point source. A point source of about 1.4 mCi/ml of $^{99m}\text{TcO}_4^-$ was positioned at the COR using the adjustment implement (Fig. 3). A pinhole insert with a diameter of 4.8 mm was employed, and the distance between the pinhole center and point source was 39.5 mm. Projection data were acquired for 120 angular views in steps of 3° . The acquisition time for each step was 15 s. Three images were reconstructed from the projection data with the 90° orbit, 45° orbit, and both the orbits using the 3D OSEM algorithm (2 iterations and 8 subsets). The matrix size of the image was $128 \times 128 \times 128$ and the voxel size was $0.76 \times 0.76 \times 0.76 \text{ mm}^3$ (zooming factor of 6.35).

Since the point source was positioned at the center of both the 90° and 45° orbits, its positions in the three images should be identical. The 3D position of the point source in each image was estimated by calculating the image center of gravity, and the estimated positions in the three images were compared.

Experiment with a line source

As described above, the misalignment of the COR could be problematic especially for two orbit data acquisition. Thus, in our system, the camera was kept fixed while the target object was rotated. For evaluating the misalignment of the COR for our system as well as the conventional system, experiments were performed using a line source phantom with an inner diameter of 1.14 mm. The phantom was filled with about 4.0 mCi of $^{99m}\text{TcO}_4^-$ solution. The phantom was carefully placed at the center in one projection view. First, the pinhole detector was rotated around the phantom with a rotation radius of 9 mm. Next, the phantom was rotated on the rotating stage. In both cases,

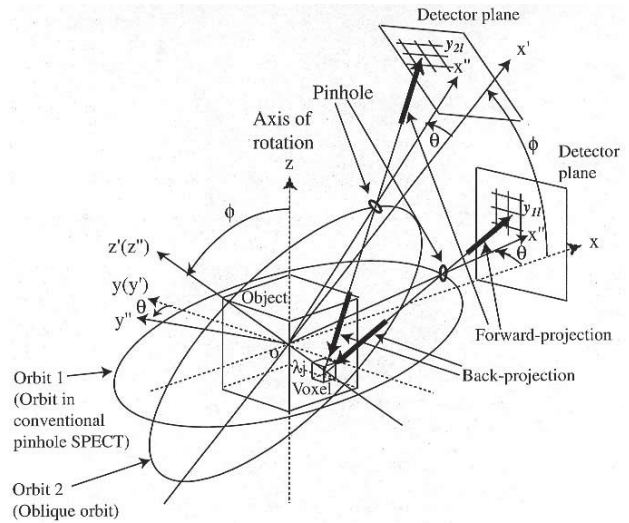


Fig. 5 Coordinate system of oblique circular orbits in pinhole SPECT with two circular orbits.

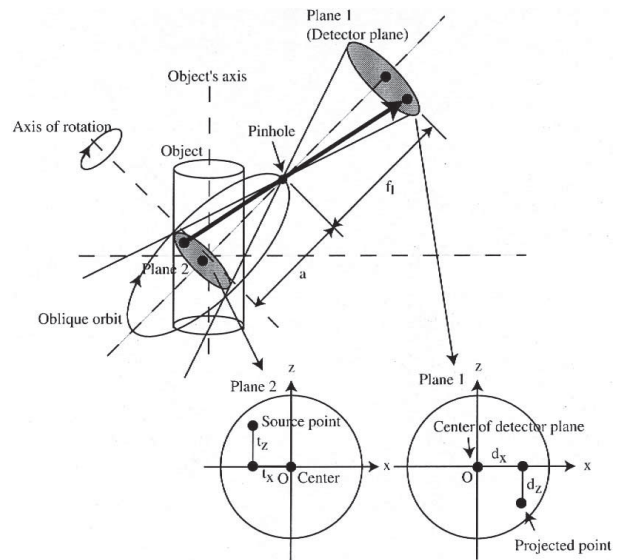


Fig. 6 Pinhole geometry for oblique orbit in pinhole SPECT with two circular orbits.

a pinhole with a diameter of 1 mm was used, and data were acquired from 120 angular views ($3^\circ/\text{view}$). The data by both systems were reconstructed using the 3D OSEM algorithm.

Animal experiment

In order to demonstrate the reconstructed image by our system, a study was performed with a rat (SD rat; body weight: 150 g) and $^{99m}\text{Tc-HMDP}$, an agent for bone scanning. $^{99m}\text{Tc-HMDP}$ was also accumulated in the bladder of the rat. Therefore, to eliminate the effect of radioactivity in the bladder, both kidneys of the rat were removed before $^{99m}\text{Tc-HMDP}$ (185 MBq/ml) was intra-

Table 1 Results of the experiment with a point source. Estimated position of the point source in the image

	x (mm)	y (mm)	z (mm)
90° orbit	0.0505	0.0511	0.0137
45° orbit	0.0464	0.0426	0.0290
both orbits	0.0643	0.0504	0.0165

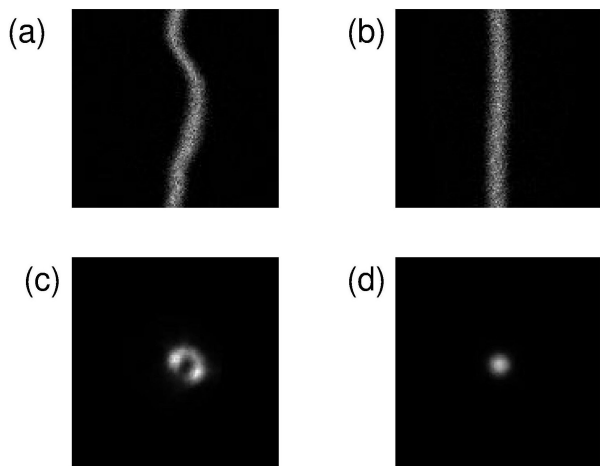


Fig. 7 Results of the experiments with the line source phantom. (a) Sinogram data measured by the conventional system (rotating the camera), (c) image reconstructed by the conventional system, (b) sinogram data measured by the proposed system (rotating the object), and (d) image reconstructed by the proposed system.

venously injected. The rat was set on the rotation unit of 90° orbit and data acquisition using the proposed system was begun 1 h after the injection. The rotation radius was 85 mm, and data were acquired from 120 angular views (3°/view) for 40 min. Subsequently, the rat was set on the rotation unit of the 45° orbit and data were acquired for 40 min. The energy window was 140 keV \pm 10%. The diameter of the pinhole insert was 1 mm. The acquired data were sent to the PC for reconstruction using the 3D OSEM algorithm with two iterations and eight subsets. For comparison, the conventional filtered backprojection algorithm (the Feldkamp FBP algorithm)⁹ was employed to reconstruct the image using the data acquired from the 90° orbit. No correction for attenuation of photons or scattered rays was made in any of the processes.

RESULTS

Experiment with a point source

Table 1 lists the estimated positions of the point source in the three reconstructed images. These three point-source positions were almost at the center (the distance from the center was 0.083 mm at maximum) and were close in value. This indicates a sufficient accuracy of intersection of the two axes and the pinhole center.

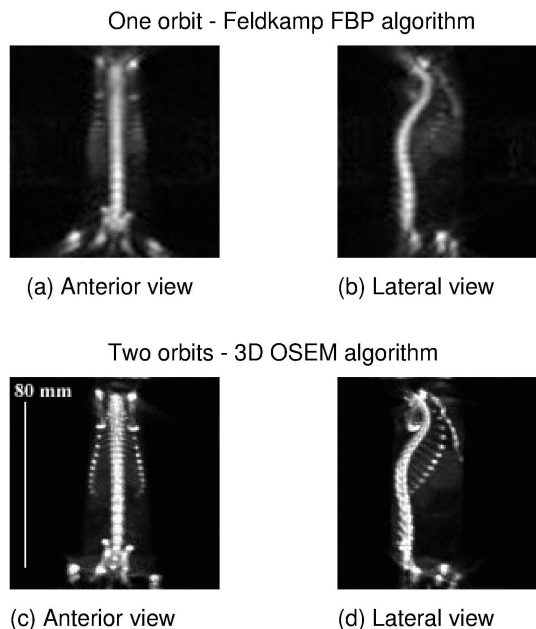


Fig. 8 Representative images of rat bone scintigrams by ^{99m}Tc-HMDP. The images of (a) and (b) were reconstructed using the Feldkamp FBP algorithm with data from the 90° orbit. The images of (c) and (d) were reconstructed using the 3D OSEM with two orbital data. All images were generated by the maximum intensity projection (MIP) method.

Experiment with a line source

Figure 7 shows the results of the experiments with a line source phantom. Misalignment of the COR was clearly observed when the camera was rotated. This results in an artifact on the reconstructed image (Fig. 7 (c)). On the other hand, no obvious artifact was observed when our system was used.

Animal experiment

Figure 8 shows the maximum intensity projection (MIP) images of the rat with ^{99m}Tc-HMDP obtained using the Feldkamp FBP algorithm with one set of orbital data and the 3D OSEM with two orbital data. The artifact of the image was significantly reduced, and a thin rib was clearly observed when data from two orbitals were used.

DISCUSSION

In this paper, we present the pinhole SPECT system for imaging small animals using data from two orbits. In the proposed system, the position of the detector is kept fixed while the target object is rotated.²² As compared with the conventional system with one orbit, our system requires a more accurate adjustment of the COR. The experiments with the point and line sources indicated that our system achieved sufficient accuracy in adjusting the COR of the two orbits. This result was apparent in the bone scan with a rat. Image distortion and axial blurring observed in the

one orbital system were greatly improved in the proposed system with two orbits.

Metzler et al. proposed the use of a helical scan system in order to acquire complete data by pinhole SPECT.²³ In the helical scan, sensitivity may be hampered when the pinhole moves across the target object. On the other hand, the sensitivity of our system is not affected since the object is positioned at the center of the field-of-view.

The system proposed in this paper is still in the prototype stage, and in order to acquire data from two orbits, the object must be moved from one orbit to the other. We plan to build a system with multiple pinhole detectors in order to increase the sensitivity.

Our final goal is to develop a system that achieves quantitative functional imaging of small animals. Although the image quality achieved by the proposed system has dramatically improved, several issues have yet to be considered for quantification. Penetrated photons at the collimator and photons scattered from the object as well as the collimator will degrade the image quality and quantity.²⁴ It is also important to consider the sensitivity compensation of the pinhole collimator when reconstructing an image.²⁵ In order to achieve a quantitative functional image using the proposed system, these issues should be rectified in the future.

CONCLUSION

We developed a pinhole SPECT system for the imaging of small animals. The proposed system consists of two axes so that complete data are acquired. Image uniformity was dramatically improved by our system. This system will provide accurate quantitative information on the biological functions of small animals.

ACKNOWLEDGMENT

This study was financially supported by the Budget for Nuclear Research of the Ministry of Education, Culture, Sports, Science and Technology, based on screening and counseling by the Atomic Energy Commission.

REFERENCES

1. Chatzioannou AF. PET scanner dedicated to molecular imaging of small animal models. *Mol Imaging Biol* 2002; 4: 47–63.
2. Tai YC, Chatzioannou AF, Yang Y, Silverman RW, Meadors K, Siegle S, et al. MicroPET II: design, development and initial performance of an improved microPET scanner for small-animal imaging. *Phys Med Biol* 2003; 48: 1519–1537.
3. Jeavons AP, Chandler RA, Dettmar CAR. A 3D HIDAC-PET camera with submillimetre resolution for imaging small animals. *IEEE Trans Nucl Sci* 1999; 46: 468–473.
4. Weber DA, Ivanovic M, Franceschi D, Strand S-E, Erlandsson K, Franceschi M, et al. Pinhole SPECT: An approach to *in vivo* high resolution SPECT imaging in small laboratory animals. *J Nucl Med* 1994; 35: 342–348.
5. Jaszczak RJ, Li J, Wang H, Zalutsky MR, Coleman RE. Pinhole collimation for ultra-high-resolution small-field-of-view SPECT. *Phys Med Biol* 1994; 39: 425–437.
6. Ishizu, K, Mukai T, Yonekura Y, Pagani M, Fujita T, Magata Y, et al. Ultra-high resolution SPECT system using four pinhole collimators for small animal studies. *J Nucl Med* 1995; 36: 2282–2287.
7. Ogawa K, Kawade T, Nakamura K, Kubo A, Ichihara T. Ultra high resolution SPECT for small animal study. *IEEE Trans Nucl Sci* 1998; 45: 3122–3126.
8. Aoi T, Watabe T, Deloar HM, Ogawa M, Teramoto N, Kudomi N, et al. Absolute quantitation of regional myocardial blood flow of rats using dynamic pinhole SPECT. Conference Record of IEEE Nuclear Science and Medical Imaging Conference 2002.
9. Feldkamp LA, Davis LC, Kress JW. Practical cone beam algorithm. *J Opt Soc Am* 1984; 29: 612–619.
10. Shepp LA, Vardi Y. Maximum likelihood reconstruction for emission tomography. *IEEE Trans Med Imag* 1982; MI-1: 113–122.
11. Lange K, Carson R. EM reconstruction algorithms for emission and transmission tomography. *J Comput Assist Tomogr* 1984; 8: 306–316.
12. Hudson HM, Larkin RS. Accelerated image reconstruction using ordered subsets of projection data. *IEEE Trans Med Imag* 1994; 13: 601–609.
13. Vanhove C, Defrise M, Franken PR, Everaert H, Deconinck F, Bossuyt A. Interest of the ordered subsets expectation maximization (OS-EM) algorithm in pinhole single-photon emission tomography reconstruction: a phantom study. *Eur J Nucl Med* 2000; 27: 140–146.
14. Tuy HK. An inversion formula for cone-beam reconstruction. *SIAM J Appl Math* 1983; 43: 546–552.
15. Grangeat O, Sire P, Guillemaud R, La V. Indirect cone-beam three-dimensional image reconstruction. In: *Contemporary Perspectives in Three-Dimensional Biomedical Imaging*, Roux C, Coatrieux JL (eds), Amsterdam; IOS Press, 1997: 29–52, 343–350.
16. Kudo H, Saito T. Feasible cone beam scanning methods for exact reconstruction in three-dimensional tomography. *J Opt Soc Am A* 1990; 7: 2169–2181.
17. Kudo H, Saito T. Derivation and implementation of a cone-beam reconstruction algorithm for nonplanar orbits. *IEEE Trans Med Imag* 1994; 13: 196–211.
18. Kudo H, Saito T. An extended completeness condition for exact cone-beam reconstruction and its application. Conference Record of IEEE Nuclear Science and Medical Imaging Conference 1994, 1710–1714.
19. Zeniya T, Watabe H, Aoi T, Kim KM, Teramoto N, Hayashi T, et al. A new reconstruction strategy for image improvement in pinhole SPECT. *Eur J Nucl Med Mol Imag* 2004; 31: 1166–1172.
20. Li J, Jaszczak RJ, Greer KL, Coleman RE. A filtered backprojection algorithm for pinhole SPECT with a displaced center-of-rotation. *Phys Med Biol* 1994; 39: 165–176.
21. Li J, Jaszczak RJ, Coleman RE. Maximum likelihood reconstruction for pinhole SPECT with a displaced center-of-rotation. *IEEE Trans Med Imag* 1995; 14: 407–409.

22. Habraken JB, de Bruin K, Shehata M, Booi J, Bennink R, van Eck Smit BL, et al. Evaluation of high-resolution pinhole SPECT using a small rotating animal. *J Nucl Med* 2001; 42: 1863–1869.
23. Metzler SD, Greer KL, Jaszczak RJ. Helical pinhole SPECT for small-animal imaging: A method for addressing sampling completeness. *IEEE Trans Nucl Sci* 2003; 50: 1575–1583.
24. Deloar HM, Watabe H, Aoi T, Iida H. Evaluation of penetration and scattering components in conventional pinhole SPECT: phantom studies using Monte Carlo simulation. *Phys Med Biol* 2003; 48: 1–14.
25. Smith MF, Jaszczak RJ. The effect of gamma ray penetration on angle-dependent sensitivity for pinhole collimation in nuclear medicine. *Med Phys* 1997; 24: 1701–1709.